The rate process of the field-induced modulated-ferroelectric phase transition in thiourea

1989 J. Phys.: Condens. Matter 1 3789

(http://iopscience.iop.org/0953-8984/1/24/003)

J. Phys.: Condens. Matter 1 (1989) 3789–3799. Printed in the UK

The rate process of the field-induced modulated–ferroelectric phase transition in thiourea

Shigeki Komori†, Shuichi Hayase and Hikaru Terauchi
Department of Physics, Kwansei-Gakuin University, Nishinomiya 662, Japan

Received 22 November 1988

Abstract. Time-resolved x-ray diffraction measurements of the electric-field-induced modulated–ferroelectric phase transition in thiourea [$SC(NH_2)_2$] have been made. When the phase changes at the transition point around $T_c = 169$ K, scaling phenomena are seen in the time evolution of the integrated intensity. In addition, the phase change proceeds along the valley of free energy in the order parameter space. This phase change of the modulated–ferroelectric transition is explained in terms of a well known nucleation and growth mechanism.

1. Introduction

The rate process of a phase change presents attractive problems. Modern understanding of this phenomenon is based on a key concept of scaling (Yamada *et al* 1984, Axe and Yamada 1986). Scaling phenomena of a phase change can be seen in many systems with first-order phase transitions (Gunton *et al* 1982), in which the time dependence of a dynamical structure function $S(k, t)$ through the phase change can be scaled onto a time evolution curve. Most scaling phenomena have been observed in processes such as the phase separation of an alloy where the time evolution of $S(k, t)$ is slow. Faster processes have not been investigated using dynamical structure analysis.

In recent years there have been dramatic developments in time-resolved x-ray diffraction techniques, so that now it is possible to observe the dynamical structure function $S(k, t)$ in considerably faster phase changes. Several investigations have been made into alloys, ferroelectrics (Yamada 1981, Komori *et al* 1985) and into inorganic compounds with reconstructive transitions (Yamada *et al* 1984). Various difficulties are of course encountered in the observations: one is the unnecessary heating or cooling by latent heat associated with a first-order transition induced by an external variable (pressure or electric field). Such heating raises the temperature of a crystal so that structural relaxation due to the temperature change takes place as well as one due to the first-order phase transition. The field-induced modulated–ferroelectric phase transition in thiourea [$SC(NH_2)_2$] is suitable for investigating the kinetics of the first-order transition by time-resolved diffractometry, because its low latent heat (28.3 J mol^{-1}) does not prevent an isothermal change from an equilibrium to a non-equilibrium state by switching on an electric field.

Intensive studies have been made of the phase transitions in thiourea and its deu-

† Present address: LSI R&D Laboratory, Mitsubishi Electric Corporation, 4-1 Mizuhara, Itami 664, Japan.

0953-8984/89/243789 + 11 $02.50

terated compound (see Denoyer and Currant 1986, and references therein). Thiourea undergoes a series of structural phase transitions at 202 K, 178.2 K, 177.4 K and 169 K with decreasing temperature (in the present sample; see also Takenaka *et al* 1979, Shiozaki 1971). Phase V, the highest temperature phase, is a normal phase with space group P*bn*m. Structural modulation with a wavevector $q_0 = (0, 0, 2\pi\delta/c)$, where $\delta \simeq 0.14$, appears at the first transition ($T_N = 202$ K) from phase V to IV. Phases IV and II† are incommensurate phases with $\delta = 0.142$–0.111. Phase III is commensurate with $\delta = \frac{1}{8}$. Phase I, the lowest temperature phase, is a commensurate phase with $\delta = 0$ and shows ferroelectric properties along the *b*-axis below $T_c = 169$ K. The I–II transition temperature increases with increasing electric field. Thus phase II just above T_c turns to phase I on the application of an electric field parallel to the *b*-axis. The associated latent heat is low enough to allow investigations of the rate process of the phase change in thiourea.

Scaling properties can be used to determine the nature of the phase change of the modulated–ferroelectric transition. The kinetics of modulated–ferroelectric transitions in some systems has been investigated using x-ray diffraction methods; Yamada (1981) reported on the field-induced lock-in transition in $NaNO_2$. Here we present the results of time-resolved x-ray measurements of the phase change in a field-induced modulated–ferroelectric transition to discuss the scaling property and the mechanism of the phase change in thiourea.

2. Experimental procedure

Single crystals of thiourea were grown by slow evaporation from a saturated methanol solution. One of the single crystals was cut into pieces 3.0 mm × 2.0 mm × 0.41 mm. Gold electrodes were deposited on the specimen with a well grown (010) plane in a vacuum, and the sample was attached to copper block by silver paste to ensure good electrical and thermal contacts.

A conventional double-axis spectrometer was employed with Cu Kα radiation from a rotating anode x-ray source giving a power of 3.2 kW (40 kV, 80 mA, focus size 0.5×5 mm^2). The radiation was monochromatised by a pyrolytic graphite crystal. For the low-temperature measurements a closed cycle cryocooler was used and the temperature of the specimen was stabilised within ± 0.1 K.

Figure 1 shows the experimental geometry. Both the (060) fundamental peak and the $(0, 6, \pm \delta)$ satellite peaks could be observed simultaneously by the one-dimensional x-ray detector (PSPC) perpendicular to the scattering plane. A block diagram of the x-ray detection system is shown in figure 2(*a*). For the time-resolved measurements, a computer-controlled multi-channel analyser (MCA) was utilised to accumulate diffraction profile data and to switch data bank memories automatically after specific time intervals (>20 μs). A high-voltage switching circuit applied high voltage to the specimen, and was synchronised with the activation of MCA. Figure 2(*b*) shows a pulse sequence of the high voltage compared with that of comb pulses for triggering the MCA.

Figure 3 shows an *E*–*T* phase diagram of the specimen just above T_c. The solid line separating the modulated and ferroelectric (non-modulated) phase represents a ferroelectric transition point under an electric field. The critical field E_c of the transition increases by 1.2 kV cm^{-1} K^{-1} with increasing temperature. Open circles in the modulated phase show initial states designated by field and temperature before the onset of the

† Strictly speaking, the incommensurate phase II undergoes the lock-in transition to a commensurate phase II′ with the modulation wavenumber $\frac{1}{8}$ at 170 K.

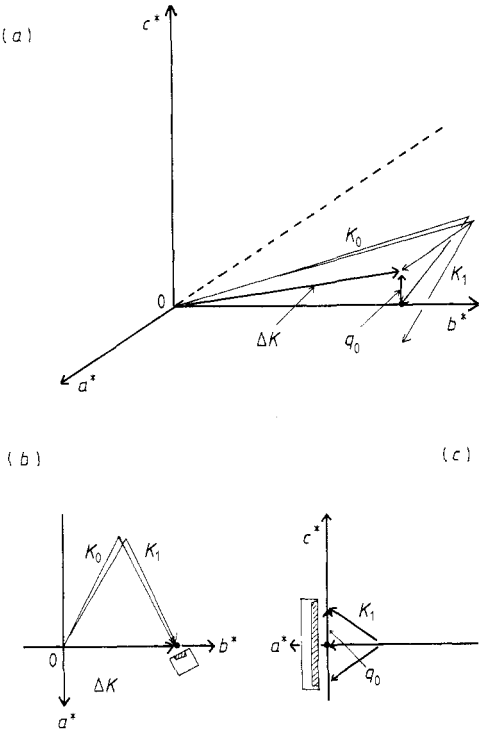

Figure 1. Experimental geometry for the measurements by use of PSPC perpendicular to the scattering plane which can detect diffraction patterns along the ⟨001⟩ direction. (*a*) Ewald representation for measurements of (060) Bragg peak and (06δ) satellite peak. ΔK and $q_0 = 2\pi\delta/c$ are wavevector transfer and modulation wavevector of the (06δ) peak. (*b*) Diffraction geometry in the a^*–b^* plane. (*c*) Diffraction geometry in the a^*–c^* plane.

electric field. Closed circles in the ferroelectric phase show the field and temperature after the isothermal onset of the electric field. These are maintained during the change in the system from a non-equilibrium to an equilibrium state. X-ray measurements were made for isothermal field jumps connecting an open circle to a closed one. Structural relaxations were observed along with changes from modulated to ferroelectric phase, after the sudden and isothermal change in the electric field. Results of the x-ray measurements on the relaxation are given in § 3.

3. Results and discussion

3.1. Time evolution of the integrated intensity

Figure 4 shows a typical time evolution of the (060) and (0, 6, $\pm$ δ) diffraction patterns at T_c + 1 K and E = 6.0 kV cm^{-1}. The integrated intensity of (060) [that of (0, 6, $\pm$ δ)] increases [decreases] after the onset of the electric field. On the other hand, no change is observed in the structural modulation wavevector and the full width at half maximum (FWHM) of the diffraction patterns through the field-induced transition.

Figure 5 shows the integrated intensity of the (060) Bragg peak as a function of time after the onset of the electric field at T_c + 1 K. The plot displays an upward curvature, and approaches the equilibrium value of the integrated intensity. The relaxation functions of

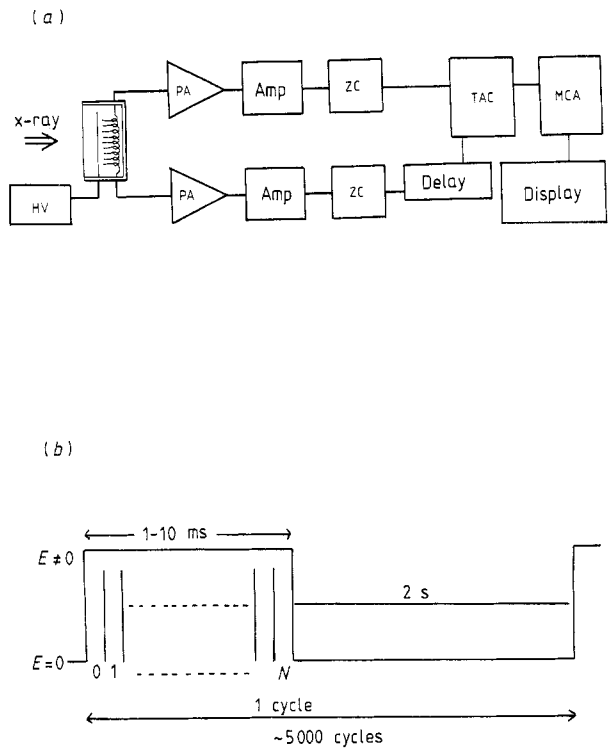

Figure 2. (*a*) Block diagram of the time-resolved x-ray detection system. PA: preamp, Amp: main amp, ZC: zero-cross detector, Delay: delay circuit, TAC: time–amplitude converter, MCA: multi-channel analyser, and HV: high-voltage supply. (*b*) Timing chart of the MCA gate circuit.

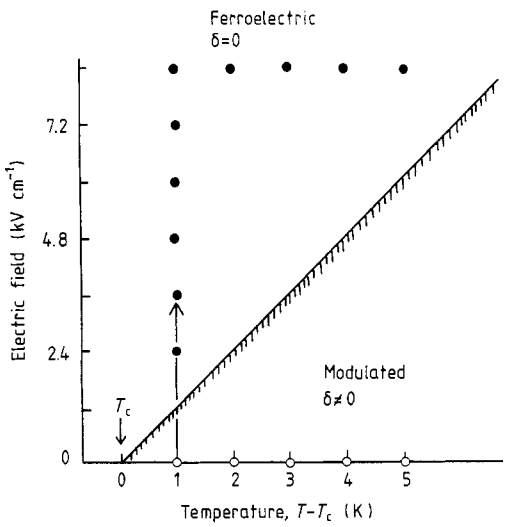

Figure 3. *E–T* phase diagram of thiourea around $T_c = 169$ K. The electric field is changed rapidly and isothermally from zero (open circles) to E ($\neq 0$) (full circles). The arrow connecting open and closed circles denotes an example of the field change.

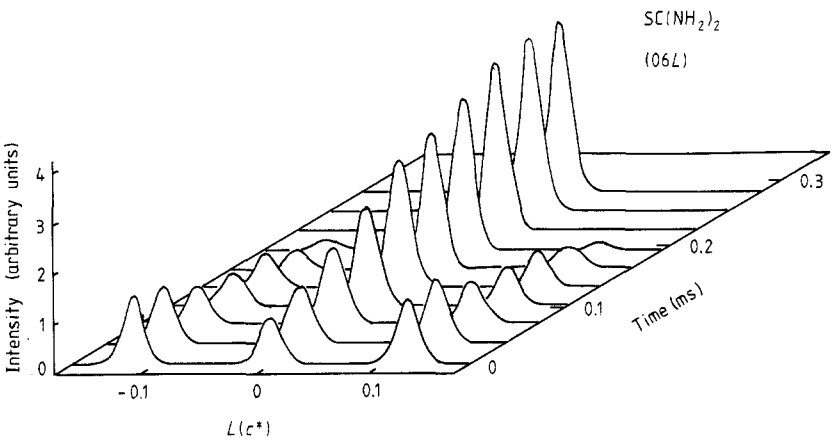

Figure 4. A typical time evolution of diffraction patterns around (060) and $(0, 6, \pm\delta)$ observed at $T_c + 1$ K and 6 kV cm^{-1}.

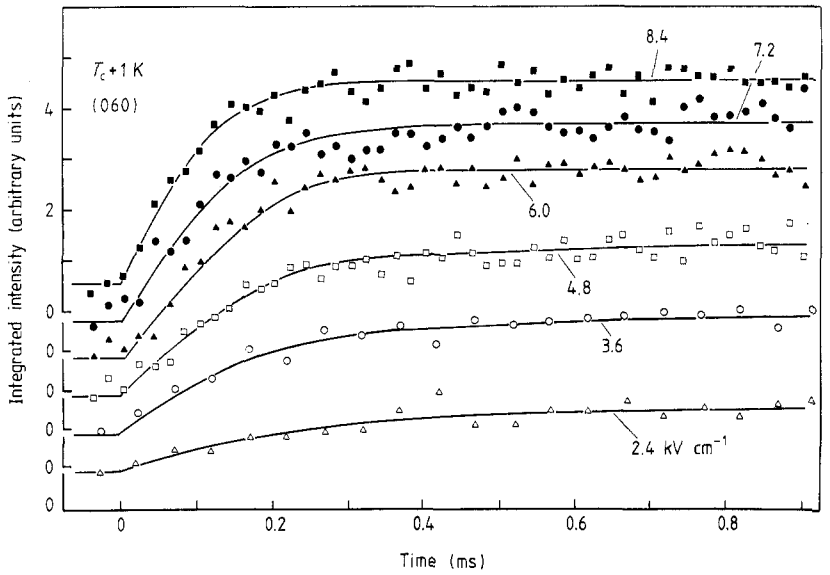

Figure 5. Time evolution of (060) integrated intensity at $T_c + 1$ K after the onset of the electric field.

the integrated intensities are well approximated by an exponential function. Another feature of the relaxation is that the rate of change in the integrated intensity increases with increases in the applied electric field.

The integrated intensity of the $(0, 6, \delta)$ satellite peaks are shown as functions of time in figure 6. The integrated intensity decreases over time and eventually approaches zero. The features of the relaxation, the exponential function of time the faster rate at greater fields, are similar to those of (060).

3.2. Scaling phenomena

The results of the exponential relaxation in § 3.1 lead to a scaling behaviour of the time evolution of the integrated intensity. Now consider the evolution function defined by

$$H(t) = (I(t) - I(0))/(I(\infty) - I(0)) \tag{1}$$

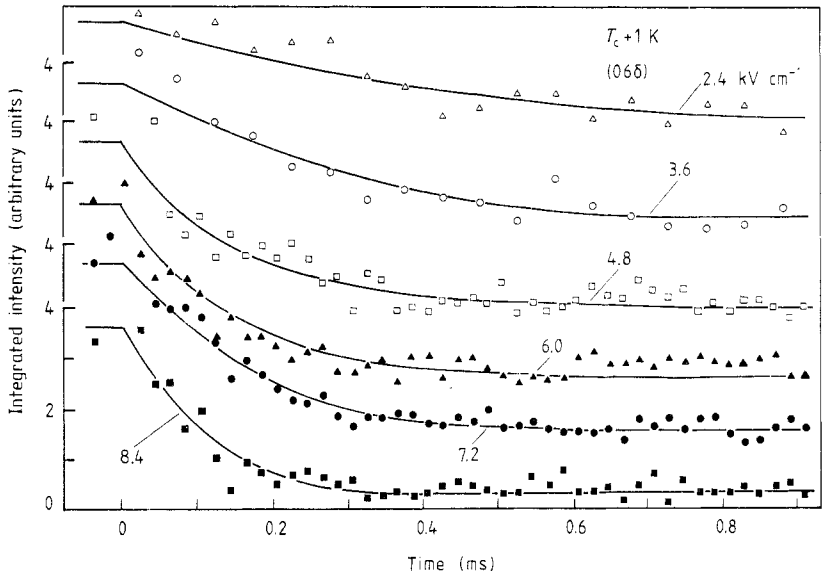

Figure 6. Time evolutions of (06δ) integrated intensity at $T_c + 1$ K after the onset of the electric field.

for (060) integrated intensity, and

$$K(t) = (I(t) - I(\infty))/(I(0) - I(\infty)) \tag{2}$$

for (06δ) integrated intensity. In these $I(t)$ is integrated intensity at time t after the onset of the electric field, E. The results in § 3.1 show that the time evolution of the integrated intensity can be described by

$$H(t, E) = 1 - \exp(-R(E)t) \tag{3}$$

and

$$K(t, E) = \exp(-R'(E)t). \tag{4}$$

According to the property of an exponential function, the time dependence of the integrated intensity is described by a universal function of time, when the half-recovery time $\tau_{1/2}$, defined by

$$H(\tau_{1/2}) = \tfrac{1}{2} \tag{1'}$$

and

$$K(\tau'_{1/2}) = \tfrac{1}{2} \tag{2'}$$

are regarded as units of time. Using $\tau_{1/2}$ and $\tau'_{1/2}$, equations (3) and (4) can be rewritten as

$$H(t/\tau_{1/2}) = 1 - \exp[-D(t/\tau_{1/2})] \tag{5}$$

$$K(t/\tau'_{1/2}) = \exp[-D(t/\tau'_{1/2})] \tag{6}$$

where D is equal to $\ln 2 (= 0.693\ldots)$.

Figure 7 shows the evolution function $H(t)$ of (060) integrated intensity versus time reduced by the half-recovery time $\tau_{1/2}$. Note that one particular scaling curve represents all of the time evolution curves of the integrated intensity; the solid line in figure 7 is

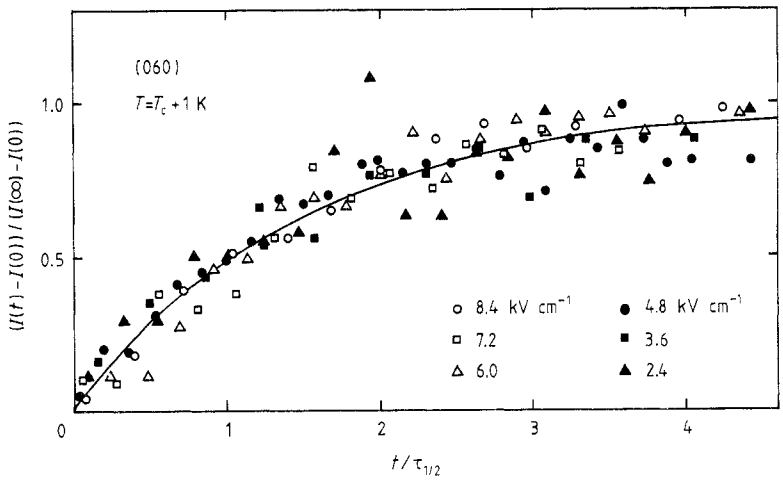

Figure 7. (060) integrated intensities versus time reduced by half-recovery time.

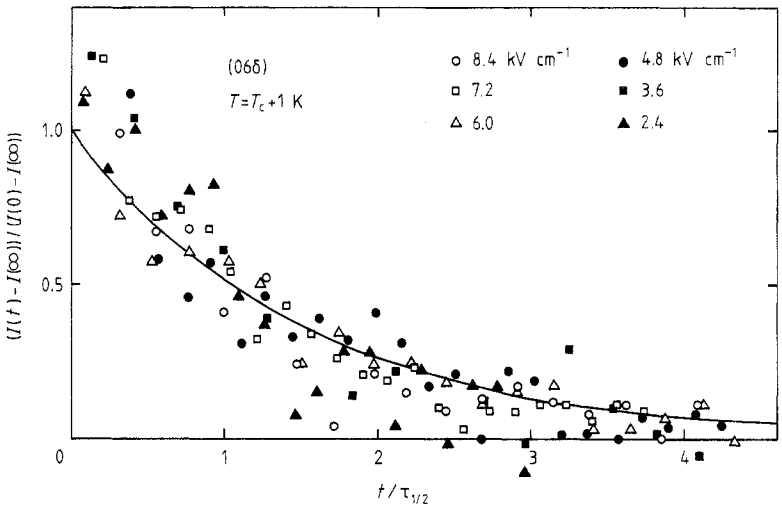

Figure 8. (06δ) integrated intensities versus time reduced by half-recovery time.

calculated from equation (5).

A similar result is obtained for the evolution of (06δ) from the plot of $K(t)$ versus $t/\tau_{1/2}$ shown in figure 8. In this case the evolution function is well represented by one scaling curve from equation (6). Thus we can rewrite equations (5) and (6) as

$$H(\tau) = 1 - \exp(-D\tau) \tag{5'}$$

$$K(\tau') = \exp(-D\tau') \tag{6'}$$

where $\tau = t/\tau_{1/2}$ and $\tau' = t/\tau_{1/2}$.

A remarkable feature of the half-recovery time can be seen in figure 9(a). The half-recovery time, i.e., a scaling factor of time, increases divergently as the field approaches a critical value E_c at $T_c + 1$ K. This feature is seen in both (060) and (06δ) evolution. This slowing down, the increase in $\tau_{1/2}$, implies an increase in the free energy change to a transition state, a saddle point of a path connecting an initial (non-equilibrium) state

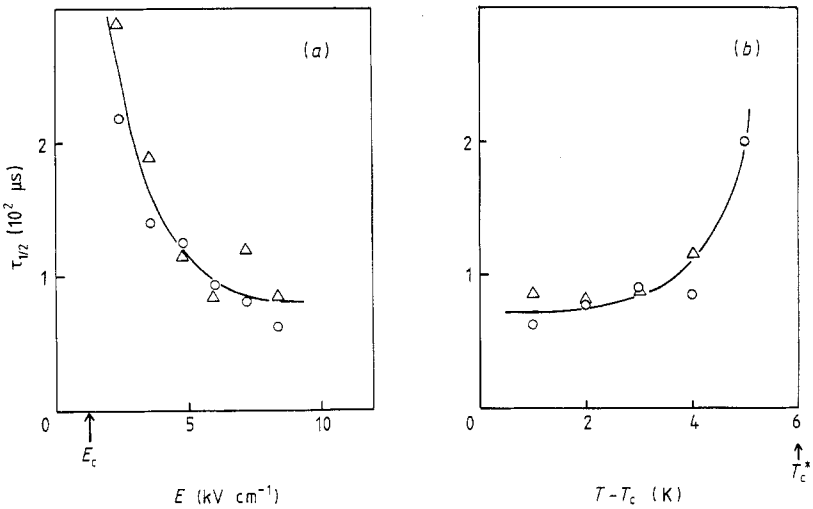

Figure 9. (*a*) Electric field dependence of the half-recovery time. E_c is the transition point of the field-induced modulated–ferroelectric transition at $T_c + 1$ K. (*b*) Temperature dependence of the half-recovery time. T_c^* is a transition point at 8.4 kV cm^{-1}.

to a final (equilibrium) state. The half-recovery time also increases divergently as the temperature approaches the critical value at 8.4 kV cm^{-1}. Figure 9(*b*) shows the temperature dependence of the half-recovery time at $E = 8.4$ kV cm^{-1}. In addition, the value of $\tau_{1/2}$ is nearly equal to that of $\tau'_{1/2}$ so that from equations (5) and (6) $H(\tau) + K(\tau)$ is approximately equal to unity.

3.3. Path of the phase change on a free energy surface in the order parameter space

Now we consider a free energy surface defined in the phase space of the order parameters ξ_0 and ξ_1 for the ferroelectric and modulated structures with wavevector q_0, respectively. The free energy density with $\xi = \xi_0 + \xi_1 \cos(q_0 z)$ can be expanded as follows:

$$f(z) = \tfrac{1}{2}(T - T_0)\xi^2 + \tfrac{1}{4}b\xi^4 + \tfrac{1}{2}c(\partial\xi/\partial z)^2 + \tfrac{1}{4}d(\partial^2\xi/\partial z^2)^2 + \tfrac{1}{2}g\xi^2(\partial\xi/\partial z)^2 - \xi_0 E \qquad (7)$$

where b, c, d and g are constants. The parameters b, d and g are obtained from the static measurements of integrated intensity, which give $b = 200$, $d = -1.27 \times 10^{-3}$ and $g = 1.62 \times 10^4$. It is assumed that $c = 1$. The free energy contours can be calculated for any pair of order parameters (ξ_0, ξ_1) using equation (7).

Figure 10 shows the free energy contours in the phase space at $T_c + 1$ K. Two minima can be seen in the free energy surface. A true minimum is around $(\xi_0, \xi_1) = (0, 0.5)$ in the equilibrium state at $E = 0$ kV cm^{-1} (see figure 10(*a*)). A metastable minimum at $E = 6.0$ kV cm^{-1}, and a true minimum is around $(\xi_0, \xi_1) = (0.7, 0)$.

When we consider time evolution of this system, there are two viewpoints (Yamada 1981): the homogeneous model and heterogeneous model. The homogeneous model assumes that the system is macroscopically homogeneous, so that the order parameter is defined by

$$\xi(q, t) = (\xi_0(t), \xi_1(t)) \qquad (8)$$

throughout the whole volume. By using this vector order parameter, we can define the

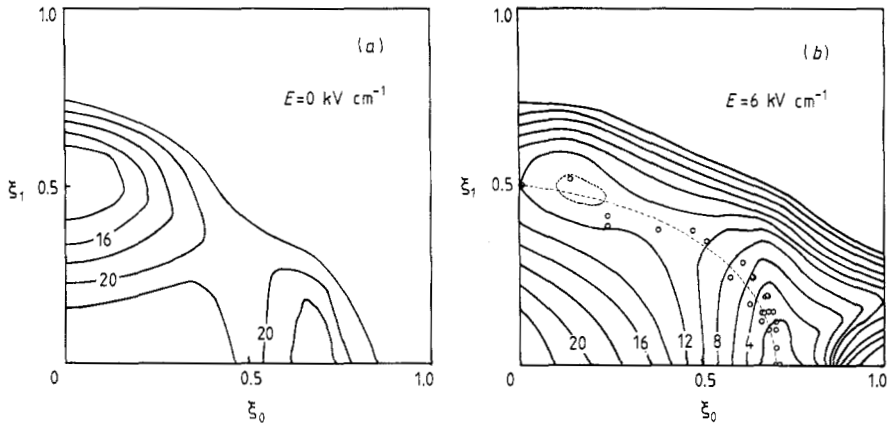

Figure 10. Free energy surface in order parameter space at $T_c + 1$ K; (*a*) $E = 0$ kV cm^{-1} and (*b*) $E = 6.0$ kV cm^{-1}.

representative point of the system in phase space. The motion of the representative point in the phase space is described by the following time-dependent Gintzburg–Landau equations:

$$-\tau_0(\partial\xi_0/\partial t) = (\partial F/\partial\xi_0) \tag{9a}$$

$$-\tau_1(\partial\xi_1/\partial t) = (\partial F/\partial\xi_1) \tag{9b}$$

and

$$F = \int f(z)\,\mathrm{d}z \tag{9c}$$

where F is the free energy, and τ_0 and τ_1 are time constants for ξ_0 and ξ_1, respectively. The integrated intensity evolution curve can be calculated by substituting equation (7) in equations (9). The result of the calculation shows that the calculated evolution curve is not described by an exponential function. Thus the homogeneous model is unsatisfactory for interpreting the time evolution of the system.

Another viewpoint is the heterogeneous model, which considers the processes of nucleation and growth. This model is based on the assumption that the system is separated into two regions, each of which is characterised by the order parameters

$$\xi(r) = \xi_0 \qquad \text{for regions of phase I} \tag{10a}$$

$$\xi(r) = \xi_1 \qquad \text{for regions of phase II.} \tag{10b}$$

Thus the time evolution of the system is due to the changes in the volume fraction of these two regions. The coordinates of the representative point in the system are defined by the vector

$$\eta(t) = (\eta_0(t), \eta_1(t)) \tag{11a}$$

with

$$\eta_0(t) = X(t)^{1/2}\xi_0 \tag{11b}$$

$$\eta_1(t) = (1 - X(t))^{1/2}\xi_1. \tag{11c}$$

After the field is turned on, the integrated intensities of (060) and (0, 6, δ) at time t

can be written as follows:

$$I(060, t) - I(060, 0) = I_0(060)X(t)\xi_0^2 \tag{12a}$$

$$I(06\delta, t) - I(06\delta, \infty) = I_0(06\delta)[1 - X(t)]\xi_1^2 \tag{12b}$$

where $X(t)$ is the volume fraction of phase I and $I(hkl, t)$ is the integrated intensity of (hkl) diffraction at time t. $I_0(hkl)$ is a constant for (hkl) reflections involving the Lorentz factor and a structure factor independent of the order parameters. Equations (12*a*) and (12*b*) are equivalent to equations (3) and (4), respectively, when $1 - \exp(-Rt)$ is substituted for $X(t)$.

From static measurements of integrated intensity, the order parameters are obtained for the initial ($t = 0$) and final ($t = \infty$) states; $(\xi_0, \xi_1) = (0, 0.5)$ at $T_c + 1$ K and 0 kV cm^{-1}, and $(\xi_0, \xi_1) = (0.7, 0)$ at $T_c + 1$ K and 6 kV cm^{-1}. Thus we can calculate $\eta_0(t)$ and $\eta_1(t)$ from the integrated intensity at time t using equations (12)–(14). The open circles in figure 10(*b*) are the coordinates of representative points. The representative point (η_0, η_1) moves through the metastable state of (0, 0.5), and reaches the equilibrium state of (0.7, 0) along a valley in the free energy surface. The trajectory of the representative point is elliptical in shape, because the coordinate (η_0, η_1) satisfies the relation

$$(\eta_0^2(t)/\xi_0^2) + (\eta_1^2(t)/\xi_1^2) = 1 \tag{13}$$

which is derived from equations (12*a*) and (12*b*). The observed representative points fall on the ellipsoid given by equation (13); this agreement between derived and observed trajectories supports the heterogeneous model.

3.4. Mechanisms of field-induced phase changes in thiourea

Here we discuss the mechanism of the phase change from the standpoint of the heterogeneous model mentioned in § 3.3.

The result of an exponential relaxation of integrated intensity can be understood by assuming that the nucleation rate is constant, the growth rate is very rapid, and the transformed region stops growing after forming a large ferroelectric aggregate. The rapid growth rate is consistent with the fact that the rate of the polarisation reversal is of the order of 10^{-7} s (McKenzie and Dryden 1973) and is much greater than the time resolution of PSPC. The assumptions of rapid growth and large ferroelectric aggregates pinned by impurities or defects in a crystal are based on the results that the FWHM remains constant throughout the transition.

Under these assumptions, the simplest evolution of the phase change is described by

$$\mathrm{d}X(t)/\mathrm{d}t = R(1 - X(t)) \tag{14}$$

where R is a rate constant and $X(t)$ is the transformed volume fraction (Avrami 1939). Thus

$$X(t) = 1 - \exp(-Rt). \tag{15}$$

$X(t)$ is equivalent to an exponential function that is well fitted to the experimental results of the intensity evolution.

In conclusion, the mechanism of the field-induced phase change from the modulated to ferroelectric phase can be described in terms of a constant nucleation rate and rapid growth.

4. Summary

X-ray diffraction measurements have been made on the field-induced modulated–ferroelectric transition near T_c in thiourea. The structural modulation wavevector $q_0 =$

$(0, 0, 2\pi\delta/c)$ ($\delta = 0.111$) and the FWHMs of the (060) and $(0, 6, \pm\delta)$ reflections remain constant through the phase change. Changes in the integrated intensity resulting from structural relaxation are described as exponential functions of time. The changes of integrated intensity are scaled onto only one curve of time evolution by using the half-recovery time which diverges as the field approaches the critical value, E_c. These facts can be understood by a physical picture of a mechanism of nucleation and growth: the ferroelectric region condenses in the para-electric region and the volume fraction of the condensed region increases with the passage of time, after the onset of the field. This mechanism is consistent with the result that the path of the phase change proceeds along the valley of the free energy surface in order parameter space.

Acknowledgments

The authors wish to express their thanks to Dr Y Noda for his illuminating discussions, and to Dr H Sakashita, Mr I Yokoyama and Mr M Nishide for their technical assistance during the course of the experiments.

References

Avrami M 1939 *J. Chem. Phys.* **7** 1103
Axe J D and Yamada Y 1986 *Phys. Rev.* B **34** 1599
Denoyer F and Currant R 1986 *Incommensurate Phases in Dielectrics* ed. R Blinc and A P Levanyuk (Amsterdam: North-Holland) pp 129–60
Gunton J D, San Miguel M and Sahni P S 1982 *Phase Transitions and Critical Phenomena* vol 8, ed. C Domb and J L Lebowitz (New York: Academic)
Komori S, Minato T, Sakashita H and Terauchi H 1985 *Japan. J. Appl. Phys.* **24** 565–7
McKenzie D R and Dryden J S 1973 *J. Phys. C: Solid State Phys.* **6** 767–73
Shiozaki Y 1971 *Ferroelectrics* **2** 245–60
Takenaka H, Terauchi H and Kawamori A 1979 *J. Phys. Soc. Japan* **46** 914–918
Yamada Y 1981 *Ferroelectrics* **35** 51–6
Yamada Y, Hamaya N, Axe J D and Shapiro S M 1984 *Phys. Rev. Lett.* **53** 1665–8